Metallicities and Temperatures for Two Metal-Rich and Two Metal-Poor Galaxies

Undergraduate Research Thesis

Presented in Partial Fulfillment of the Requirements for graduation "with Honors Research Distinction in Astronomy" in the undergraduate colleges of The Ohio State University

By

Denise Hung

The Ohio State University

May 2015

Project Advisors: Dr. Kevin Croxall & Prof. Richard Pogge, Department of Astronomy

Abstract

We observed H II regions in the star-forming galaxies IC 342, NGC 855, I Zw 18, and DDO 53 with the Multi-Object Double Spectrograph (MODS1) on the Large Binocular Telescope (LBT) to measure their gas-phase oxygen, nitrogen, argon, sulfur, and neon abundances. By detecting at least one temperature-sensitive auroral line in the optical range ([O III] λ4363Å , [N II] λ5755Å , [S III] λ6312Å , or [O II] $\lambda\lambda$7320,7330Å), we can measure "direct" gas-phase abundances for the H II regions in our sample. We can also use the strong-line ratios to infer a trend in metallicity and temperature as a point of reference for our measurements. We selected the galaxies in our sample to take advantage of new far-infrared data from Herschel Far-Infrared Space Telescope taken as part of the Key Insights on Nearby Galaxies: a Far-Infrared Survey with Herschel (KINGFISH). This permits the measurement of the [O III] λ88 μm fine-structure line, which is relatively insensitive to temperature and can be used with the temperature-sensitive [O III] λ5007Å emission line to more tightly constrain temperature estimates than the weak auroral lines. We find oxygen abundances generally in agreement with previously reported results in the literature, and temperatures consistent with those metallicities.

Chapter 1: Introduction

The elements heavier than helium, which in astronomy are all referred to as metals, play a key factor in influencing many of a galaxy's internal physical processes. Metals can alter opacities and drive various heating and cooling processes, and are connected to determining the fundamental structure of the interstellar medium (ISM) and stars. The amount of metals present in a galaxy can therefore be useful in differentiating between evolutionary paths and provides a necessary component for constraining models of chemical evolution and enrichment.

Gas-phase metal abundances in galaxies are measured using the spectra of H II regions, ionized gas clouds excited by ionizing photons ($h\nu \geq 13.6$ eV) from hot, young stars. The traditional methods use strong collisionally-excited optical emission lines that arise from ionized oxygen in the H II regions. The relative strengths of these lines depend upon the electron density (n_e), the electron temperature (T_e), and the fraction of atoms in each ionic state of the gas in the H II region. Using what is known as the "direct method" (Dinerstein 1990), measurements of temperature-sensitive auroral emission lines give estimates of the electron temperature of the ionized gas (Osterbrock & Ferland 2006). However, these lines are inherently weak and difficult to detect. The [O III] λ4363Å line has historically been the most studied of the temperature-sensitive auroral lines due to its relative ease of detection and abundance of emitting ions (e.g., Berg et al. 2015), and thus provides the best direct estimates of the electron temperature in the O^{++} ionized zone. The [O III] λ4363 line is, however, particularly weak in metal-rich H II regions, where the increased presence of metals leads to increased cooling and lower temperatures, thereby decreasing its strength. Its use in estimating the temperature is thus limited to hotter metal-poor H II regions.

In lieu of detecting the temperature-sensitive auroral lines, we may also determine gas-phase abundances through what are collectively known as the "strong-line methods" (e.g., Dopita et al. 2000). These methods do not independently measure an electron temperature and thus they rely on either empirical calibrations (e.g., Pilyugin & Thuan 2005) or theoretical methods based on photoionization models (e.g., Kobulnicky & Kewley 2004). This leads to highly discrepant metallicity estimates when compared to each other (e.g., Bresolin et al. 2004; Garnett et al. 2004, Kewley & Ellison 2008), primarily due to the different underlying assumptions and biases of each calibration method. While an absolute calibration of the strong-line methods has proved difficult to implement, we can use these techniques to determine reliable relative abundances.

Even when we are able to detect auroral lines, temperatures derived are only representative of a luminosity weighted average temperature. Different ions are not completely co-spatial. Each temperature is thus only representative of the area where that ion is found. More complex models of H II regions, such as those where we do not force the H II region to be isothermal (Peimbert 1967), suggest that the direct method may underestimate the true oxygen abundance. The far-infrared [O III] $\lambda 88\,\mu$m fine-structure emission line, however, is particularly useful as its strength is relatively insensitive to temperature, making it useful in deriving an oxygen abundance that is not as dependent on the derived temperature. Cooling contributions from far-infrared fine-structure lines become more significant as metallicity increases, particularly above an oxygen abundance of 12+log(O/H) $\sim$ 8.4, and temperature decreases (Stasińska 2002). As they have low excitation temperatures, the far-infrared emission will be emitted in the presence of doubly ionized oxygen. The [O III] $\lambda 88\,\mu$m and [O III] λ5007Å lines give us two strong lines, rather than one strong and one weak, from different energy levels to determine a temperature at a high metallicity range.

The far-infrared $88\,\mu$m line has seen limited use as it can only be measured from space or upper atmosphere telescopes, though the latter is more challenging. The Herschel Space Observatory's Photodetector Array Camera and Spectrometer (PACS) instrument allows us to observe the far-infrared [O III] lines in nearby

galaxies. We seek to uniformly calculate the abundances spanning the parameter space occupied by star-forming galaxies to enable a uniform calibration of metal abundance at both low and high metallicity. In order to make full use of the newly obtained far-infrared data, our sample consists of three galaxies selected from its recent KINGFISH project (Key Insights on Nearby Galaxies: a Far-Infrared Survey with Herschel; Kennicutt et al. 2011), chosen based on their expected range of metallicities from the mass-metallicity relation: two metal-rich and one metal-poor galaxies. We chose our fourth galaxy, I Zw 18, on the basis of it being very metal poor to help bracket the relevant parameter space. Though I Zw 18 was not specifically observed with KINGFISH, we obtained our far-infrared data for it and DDO 53 from a later Herschel program. When combined with ground-based visible-light ionized oxygen emission-line measurements, we can get a complete picture of the excitation state of the O^{++} and O^{+} ions, and derive more accurate total oxygen abundances.

We present here new oxygen, nitrogen, sulfur, argon, and neon abundance and temperature estimates for four galaxies, IC 342, NGC 855, I Zw 18, and DDO 53, by combining optical and infrared observations. IC 342 and NGC 855 are galaxies with large stellar masses, so we expect from the mass-metallicity relation (Tremonti et al. 2004) that they would also be metal-rich. Likewise, we expect the low-mass galaxies I Zw 18 and DDO 53 to be metal-poor. Our optical observations and data processing are described in Chapter 2. The electron temperatures, densities, and derived abundances are presented in Chapter 3. A discussion of the implications of our findings is given in Chapter 4.

Galaxy	α_{J2000}	δ_{J2000}	Type	Redshift	Diameter (D_{25}) arcmin	kpc	log[Stellar Mass ($M_\odot$)]
IC 342	03:46:48.503	+68:05:46.92	SAB(rs)cd	0.000103 ± 0.000010	21.4	24.42	9.95[a]
NGC 855	02:14:03.493	+27:52:38.43	E	0.001975 ± 0.000017	2.6	8.05	8.67[b]
I Zw 18	09:34:02.02	+55:14:28.1	cI;BCG	0.002505 ± 0.000007	0.3	1.62	7.95[c]
DDO 53	08:34:07.20	+66:10:54.0	Im	0.000067 ± 0.000001	1.5	1.73	6.35[d]

Table 1.1. Selected characteristics of the four galaxies in our sample. The stellar masses for IC 342, NGC 855, and DDO 53 were provided by Kennicutt et al. 2011. The stellar mass for I Zw 18 is courtesy of Fisher et al. 2014. All other data were courtesy of the NASA/IPAC Extragalactic Database (NED). Right acension and declination are in units of hours, minutes, and seconds and degrees, arcminutes, and arcseconds respectively. In cases where more than one physical major axis was reported, we referenced the most recently reported value.

Distance References—(a) Saha et al. 2002; (b) Tonry et al. 2001; (c) Aloisi et al. 2014; (d) Dalcanton et al. 2009.

Chapter 2: Observations

2.1. Optical Spectroscopy

We obtained our optical spectra with the Multi-Object Double Spectrographs (MODS, Pogge et al. 2010) on the Large Binocular Telescope (LBT) in 2013. IC 342 and NGC 855 were observed in October, and I Zw 18 and DDO 53 the following December. As both spectrographs were not available at the times of observation, all of the spectra were acquired using only MODS1. Blue and red spectra were obtained simultaneously using the G400L (400 lines mm^{-1}, R $\approx$ 1850) and G670L (250 lines mm^{-1}, R$\approx$2300) gratings, respectively. In each case, our setup allowed us to obtain a broad optical range from 3100 to 10000 Å. For each galaxy, we used a 60″ by 1.″2 slit size to take two 900s exposure observations at four neighboring positions, encompassing a total area 4.″8 wide. We then combined each pair of images for a total exposure time of 1800s, helping facilitate detection of the intrinsically weak auroral lines such as [N II] λ5755Å and [S III] λ6312Å. Given the expected high metallicities for IC 342 and NGC 855, we did not expect to detect the [O III] λ4363Å auroral line for those galaxies using these exposure times.

We will summarize the salient points of our data reduction process here, but a more detailed description of the procedures can be found in Berg et al. (2015) and Croxall et al. (2015). We reduced and analyzed our spectra using the beta version of the MODS reduction pipeline, written to run within the XIDL reduction package. We used G191-B2B as the flux standard for IC 342 and NGC 855, and respectively Hz44 and Feige 34 for I Zw 18 and DDO 53. For each slit position, we extracted the central brightest 10″ region in five equally sized subdivisions, so our total extraction area was 10″ by 4.″8 divided into twenty 2″ by 1.″2 regions. This allowed us to obtain

a more complete composite profile of each galaxy and permit us to investigate any fluctuations in metallicity or temperature across the observed area.

2.2. Spectral Modelling and Line Intensities

As light from a galaxy reaches Earth, the photons are scattered away or absorbed by the dust and gas in their path in a process known as extinction. This extinction is more pronounced at short wavelengths, leading to a loss of blue light and a "reddened" image as observed on Earth. As we are especially concerned with the ratios of lines at different wavelengths, we need to use a reddening law to correct for this effect to ensure our emission-line measurements are accurate. The Balmer series of hydrogen spectral line emissions offer a well-known standard of relative strengths. We corrected the reddening by using a Calzetti et al. (2000) law and the ratios of the intensities of the three strongest Balmer lines, Hα/Hβ, Hα/Hγ, and Hβ/Hγ. Similarly, we must also subtract the continuum of starlight from our spectra. An inaccurate model can be particularly troublesome for measuring the weak auroral lines, which may be indistinguishable from the stellar continuum. We modelled the underlying stellar continuum of the MODS1 spectra using version 04 of the STARLIGHT spectral synthesis code (Cid-Fernandes et al. 2005). We modelled our stellar continuum using stellar population models from Bruzual & Charlot (2003) that span a range of age, metallicity, and mass. We did not include more of these models as doing so greatly increased the processing time while not noticeably improving our models.

After correcting for the reddening and subtracting the stellar continuum, we initially assumed Gaussian profiles for each of our emission lines when applying the automated fit. Some emission lines were very sensitive to the modeled stellar continuum. In these cases, stellar population models were fit to provide a robust local continuum correction. Often, this restricted approach was not enough for STARLIGHT to properly distinguish the continuum from the intrinsically weak auroral lines. This was particularly true for [N II] λ5755Å, as it is located in the region of the continuum susceptible to distortion by the MODS dichroic. In these cases, we would validate the measurements of the emission lines by hand using

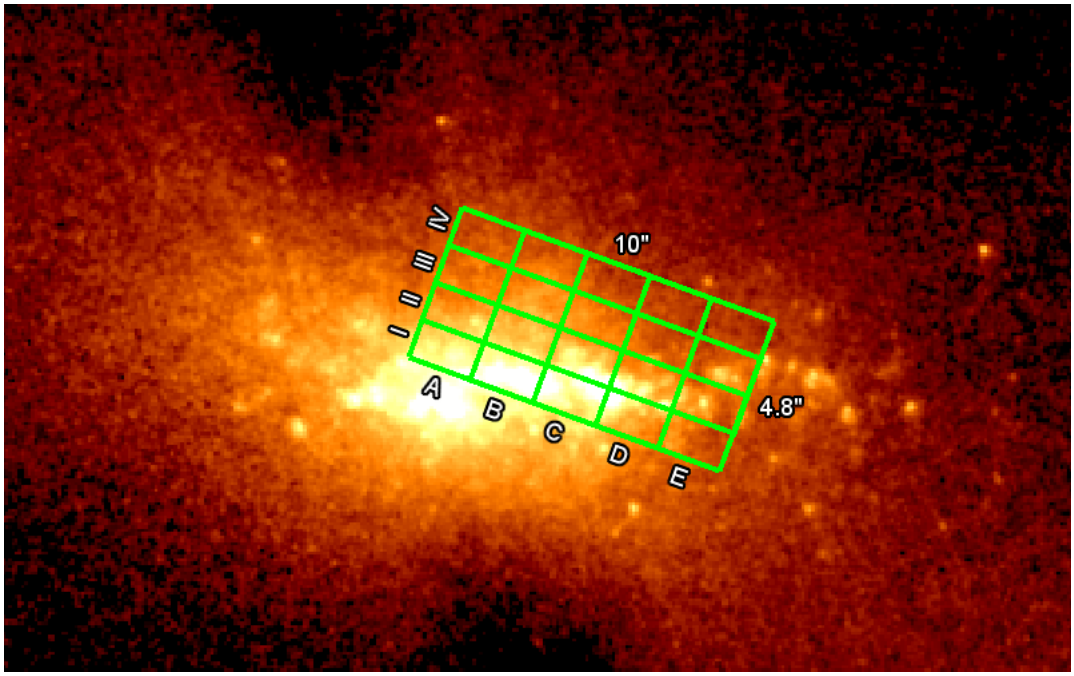

Fig. 2.1.— An example of our area of extraction for NGC 855. Photo courtesy of the Hubble Space Telescope.

SPLOT routine in IRAF. A more complete account of the continuum modeling and line fitting process may again be found in Berg et al. (2015).

To obtain the spectra for the entire $10''$ by $4\farcs8$ area of extraction, we combined the extracted spectra of each region. We then performed the automatic fit and same checks as we did on the individual spectra.

Chapter 3: Results

3.1. Deriving Density and Temperature

3.1.1. Using Optical Spectra

We cannot determine elemental abundances alone through the emission-line strengths, as they may only be conveying the luminosity of the H II region. By using the electron density (n_e) and electron temperature (T_e) of the ionized gas, as well as a correction factor for the fraction of unobserved ionic states, we can calculate the abundance of oxygen relative to hydrogen using the ratios of lines of the appropriate species. If we detect the auroral lines, we follow the same methodology described by Osterbrock & Ferland (2006), where the ratio of these lines with the stronger emission lines from the same ionized state are highly sensitive to electron temperature.

In order to find the electron density, we use the [S II] λ6717/λ6731 line ratio. These strong lines have the advantage of being easy to measure as they are well separated. We can additionally use the [O II] λ3729/λ3726 ratio, while blended at the resolution of MODS, as a point of reference for our n_e estimates. For increasing density, the strength of [S II] λ6731Å line increases relative to the [S II] λ6717Å line. The low density regime represented by an [S II] ratio of I(λ6717)/I(λ6731) $>$ 1.35 (Croxall et al. 2015). We observed this for all of our regions in NGC 855 and the majority of regions in I Zw 18 and DDO 53. As our method for finding electron density loses sensitivity at this low density limit, we adopt an n_e value of 100 cm^{-3} for these regions.

We can represent the temperature structure of the H II regions with a model separated into three ionization zones as described in Croxall et al. (2015) Temperatures may be derived from [O II], [N II], and [S II] in the low zone, [S III] and [Ar III] in the intermediate zone, and [O III] and [Ne III] in the high zone. We use T[N II], T[S III], and T[O III] as our standard temperature for each zone respectively as those correspond to the auroral lines we examined.

If we detect at least one auroral line from any one of these zones, we can convert our temperatures from one zone to another by using scaling relations described by Garnett (1992):

$$T[\text{N II}] = T[\text{O II}] = T[\text{S II}] = 0.70\ T[\text{O III}] + 3000\text{K}$$

$$T[\text{S III}] = 0.83\ T[\text{O III}] + 1700\text{K}$$

We focused our study on four temperature-sensitive ratios using the auroral lines: [O III] I(λ4959+5007)/I(λ4363), [N II] I(λ6548+6583)/I(λ5755), [S III] I(λ9069+9532)/I(λ6312), and [O II] I(λ7320+7330)/I(λ3726+3628). We expect to detect [O III] λ4363Å in hotter metal-poor H II regions, while we anticipate seeing [N II] λ5755Å and [S III] λ6312Å in cooler metal-rich regions. When measuring the weak auroral lines, we require the strength of a line to be at least three times greater than its surrounding continuum noise in order to consider it a valid detection. We check this with a visual inspection of the spectra with its continuum model. Our auroral line detections for each of our regions are compiled in Table 3.1. If we do not find a significant detection of any auroral line, such as in the case of two areas of DDO 53 (C I and D I), we will not be able to find corresponding temperature estimates or metallicities using the direct method. As we expect, we see the presence of [O III] λ4363 overwhelmingly in I Zw 18 and DDO 53 and not at all in IC 342. That we detect [O III] λ4363 in most of our NGC 855 regions, though much less pronounced in relative strength than in I Zw 18 or DDO 53, is evidence that NGC 855 is hotter and less metal-rich than IC 342.

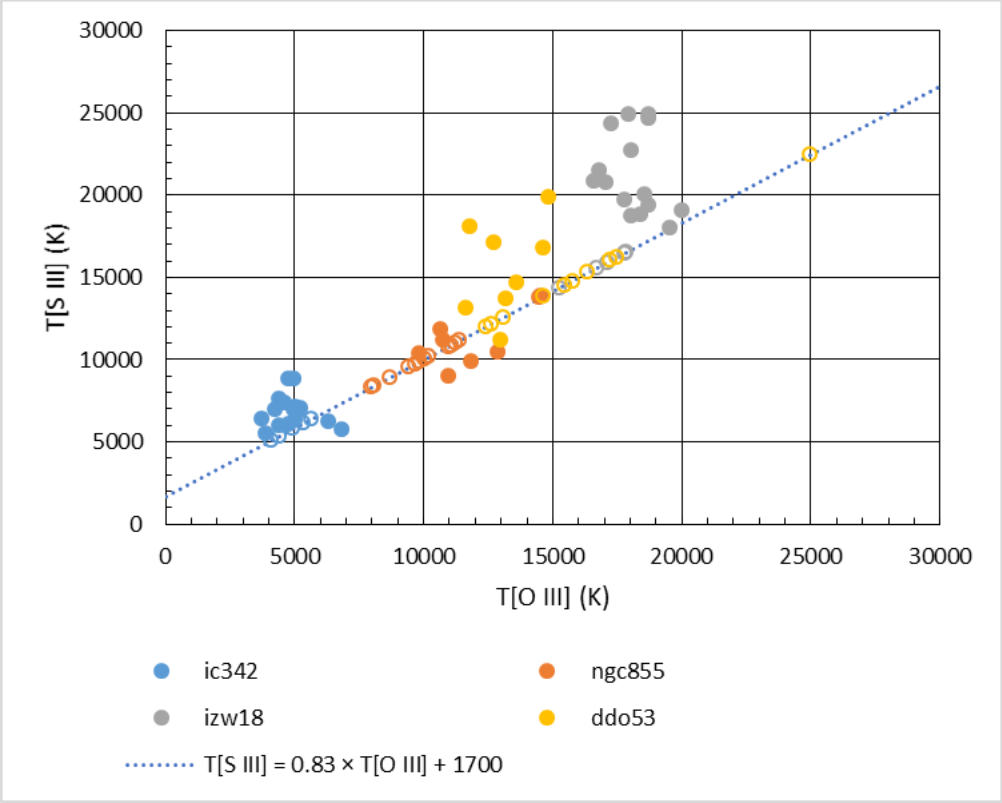

Fig. 3.1.— Plot of the T[O III] and T[S III] estimates found for every region of our galaxies alongside their scaling relations. The points where only one auroral line was used to calculate the temperature are denoted with hollow circles. As [O II] λ7320,7330 and [O III] λ4363 were almost never detected together, T[O II] and T[O III] were overwhelmingly calculated using the appropriate Garnett relation.

Galaxy	Region	α_{J2000}	δ_{J2000}	[O III]λ4363	[N II]λ5755	[S III]λ6312	[O II]λ7320,30
IC 342	A I	03:46:48.004	+68:05:43.60		√		√
	B I	03:46:48.097	+68:05:45.53		√	√	√
	C I	03:46:48.189	+68:05:47.47		√	√	√
	D I	03:46:48.282	+68:05:49.40		√	√	√
	E I	03:46:48.374	+68:05:51.33		√	√	√
	A II	03:46:48.211	+68:05:43.29		√	√	√
	B II	03:46:48.304	+68:05:45.22		√	√	
	C II	03:46:48.396	+68:05:47.15		√		
	D II	03:46:48.489	+68:05:49.09		√		√
	E II	03:46:48.581	+68:05:51.02		√		√
	A III	03:46:48.419	+68:05:42.98		√	√	√
	B III	03:46:48.511	+68:05:44.91		√	√	
	C III	03:46:48.604	+68:05:46.84		√	√	
	D III	03:46:48.696	+68:05:48.78		√	√	√
	E III	03:46:48.789	+68:05:50.71		√	√	√
	A IV	03:46:48.626	+68:05:42.67		√		√
	B IV	03:46:48.718	+68:05:44.60		√	√	√
	C IV	03:46:48.811	+68:05:46.53		√	√	√
	D IV	03:46:48.903	+68:05:48.47		√	√	√
	E IV	03:46:48.996	+68:05:50.40		√	√	√

(cont'd)

Table 3.1. MODS Observations and Auroral Line Detections

Table 3.1—Continued

Galaxy	Region	α_{J2000}	δ_{J2000}	[O III]λ4363	[N II]λ5755	[S III]λ6312	[O II]λ7320,30
I Zw 18	A I	09:34:01.700	+55:14:25.56	√			
	B I	09:34:01.854	+55:14:27.07	√		√	
	C I	09:34:02.007	+55:14:28.58	√		√	√
	D I	09:34:02.160	+55:14:30.09	√		√	
	E I	09:34:02.314	+55:14:31.60	√			
	A II	09:34:01.806	+55:14:24.77	√			
	B II	09:34:01.960	+55:14:26.28	√		√	
	C II	09:34:02.113	+55:14:27.79	√		√	√
	D II	09:34:02.266	+55:14:29.30	√		√	
	E II	09:34:02.420	+55:14:30.81	√			
	A III	09:34:01.912	+55:14:23.99	√			
	B III	09:34:02.065	+55:14:25.50	√		√	
	C III	09:34:02.219	+55:14:27.01	√		√	√
	D III	09:34:02.372	+55:14:28.52	√		√	
	E III	09:34:02.526	+55:14:30.03	√			
	A IV	09:34:02.018	+55:14:23.20	√			
	B IV	09:34:02.172	+55:14:24.71	√		√	
	C IV	09:34:02.325	+55:14:26.22	√		√	√
	D IV	09:34:02.478	+55:14:27.73	√		√	
	E IV	09:34:02.632	+55:14:29.24	√			

(cont'd)

Table 3.1—Continued

Galaxy	Region	α_{J2000}	δ_{J2000}	[O III]λ4363	[N II]λ5755	[S III]λ6312	[O II]λ7320,30
NGC 855	A I	02:14:03.570	+27:52:36.29		√	√	√
	B I	02:14:03.712	+27:52:36.97		√	√	√
	C I	02:14:03.854	+27:52:37.65	√	√	√	√
	D I	02:14:03.995	+27:52:38.34	√	√	√	√
	E I	02:14:04.137	+27:52:39.02	√	√	√	√
	A II	02:14:03.601	+27:52:35.16	√	√	√	√
	B II	02:14:03.743	+27:52:35.84	√	√	√	√
	C II	02:14:03.884	+27:52:36.52		√	√	√
	D II	02:14:04.026	+27:52:37.21			√	√
	E II	02:14:04.168	+27:52:37.89			√	√
	A III	02:14:03.632	+27:52:34.03		√	√	√
	B III	02:14:03.773	+27:52:34.71		√	√	√
	C III	02:14:03.915	+27:52:35.39	√	√	√	√
	D III	02:14:04.057	+27:52:36.08	√	√	√	√
	E III	02:14:04.199	+27:52:36.76	√	√	√	√
	A IV	02:14:03.663	+27:52:32.90	√	√	√	√
	B IV	02:14:03.805	+27:52:33.59	√	√	√	√
	C IV	02:14:03.946	+27:52:34.27	√		√	√
	D IV	02:14:04.088	+27:52:34.95	√		√	√
	E IV	02:14:04.230	+27:52:35.63	√		√	√

(cont'd)

Table 3.1—Continued

Galaxy	Region	α_{J2000}	δ_{J2000}	[O III]λ4363	[N II]λ5755	[S III]λ6312	[O II]λ7320,30
DDO 53	A I	08:34:07.466	+66:10:57.80	$\surd$			$\surd$
	B I	08:34:07.563	+66:10:55.89	$\surd$		$\surd$	$\surd$
	C I	08:34:07.659	+66:10:53.98				
	D I	08:34:07.755	+66:10:52.07				
	E I	08:34:07.852	+66:10:50.15	$\surd$		$\surd$	$\surd$
	A II	08:34:07.277	+66:10:57.45	$\surd$			$\surd$
	B II	08:34:07.373	+66:10:55.54	$\surd$			$\surd$
	C II	08:34:07.470	+66:10:53.62	$\surd$			$\surd$
	D II	08:34:07.566	+66:10:51.71	$\surd$		$\surd$	$\surd$
	E II	08:34:07.663	+66:10:49.80	$\surd$			$\surd$
	A III	08:34:07.087	+66:10:57.10	$\surd$			$\surd$
	B III	08:34:07.184	+66:10:55.19	$\surd$		$\surd$	$\surd$
	C III	08:34:07.280	+66:10:53.27	$\surd$		$\surd$	$\surd$
	D III	08:34:07.377	+66:10:51.36	$\surd$		$\surd$	$\surd$
	E III	08:34:07.473	+66:10:49.45	$\surd$			$\surd$
	A IV	08:34:06.898	+66:10:56.75	$\surd$			$\surd$
	B IV	08:34:06.994	+66:10:54.84	$\surd$			$\surd$
	C IV	08:34:07.091	+66:10:52.92	$\surd$			$\surd$
	D IV	08:34:07.187	+66:10:51.01	$\surd$			$\surd$
	E IV	08:34:07.284	+66:10:49.10	$\surd$			$\surd$

3.1.2. Using the Far-Infrared Emission Line

The far-infrared [O III] $\lambda 88\,\mu$m fine-structure line is relatively insensitive to temperature. We can use it by itself to find a robust measure of O^{++}/H^{+} that is insensitive to temperature given its low excitation energy. As as a ratio with [O III] $\lambda 5007$, it additionally gives a temperature dependent on the electron density that is necessary for finding the O^{+}/H^{+} ratio. As it has a low excitation temperature, [O III] $\lambda 88\,\mu$m is especially useful in metal-rich H II regions that do not have the advantage of a well-constrained T[O III] measurement from the [O III] $\lambda 4363$ line. We can use temperature estimates found through this method as a point of comparison for temperatures found using the direct method.

As the Herschel data were acquired using a circular beam, we measure the flux for the [O III] $\lambda 88\,\mu$m line with a circular aperture $5''$ in radius. Since the Herschel and MODS1 apertures were of different sizes, we need to use a correction factor on the [O III] $\lambda 88\,\mu$m line to obtain a proper ratio with the [O III] $\lambda 5007$ flux in the $10''$ by $4\farcs8$ area of our optical data. To obtain this factor, we look at the [O III] $\lambda 88\,\mu$m flux in the smaller MODS1 aperture and divide it by the [O III] $\lambda 88\,\mu$m flux in the circular aperture. Because of the limited resolution of the Herschel data and the far-infrared line's resistance to temperature fluctuations, we only found the [O III] $\lambda 88\,\mu$m flux for total combined spectra of each galaxy, rather than for the individual regions.

We measured the temperatures and densities for each of our regions, as well as the total combined spectra of each galaxy. Our reported values can be found in Tables 3.2 and 3.3.

3.2. Gas-Phase Abundances

Our metallicities found using the auroral lines are reported in Figure 3.2 and Table 3.4. These correspond with the electron densities and temperatures found using the direct method in Section 3.1.1.

	IC 342	NGC 855	I Zw 18	DDO 53
$T_{O\,II}$ (K)	5800 ± 500	9900 ± 1300	15400 ± 500	12400 ± 600
$T_{S\,III}$ (K)	6300 ± 500	10400 ± 1400	20000 ± 1000	12300 ± 1500
$T_{O\,III}$ (K)	4000 ± 500	10700 ± 500	18200 ± 500	13800 ± 800
n_e (cm^{-3})	764 ± 215	100 ± 100	100 ± 100	100 ± 100

Table 3.2. Temperatures and densities measured for the total combined spectra for NGC 855, I Zw 18, and DDO 53. For IC 342, we found only five regions (B I, C I, A IV, C IV, and E IV) to have plausible oxygen abundances ($12 + \log(O/H) \geq 8.7$), so we made our measurements for the total galaxy from the summation of the emission-line fluxes from those regions.

	IC 342	NGC 855	I Zw 18	DDO 53
$\lambda 88\mu m/\lambda 5007$Å	0.332 ± 0.010	0.194 ± 0.010	0.050 ± 0.156	0.010 ± 0.220
n_e (cm^{-3})	800	100	100	100
$T_{O\,III}$ (K)	6950 ± 50	11000 ± 230	···	···

Table 3.3. The n_e values used here are the same ones found using the [S II] $\lambda 6717/\lambda 6731$ ratio in Table 3.2 rounded to the nearest hundred. As the derived temperature increases for lower densities, it's best to treat the temperatures we find for our low density galaxies NGC 855, I Zw 18, and DDO 53 as an upper bound.

Additionally, we can use certain strong-line ratios to find relative abundances. Although an absolute calibration for metallicities obtained through the strong-line methods remains uncertain (Kewley & Ellison 2008), we may still use the strong-line ratios to illustrate and check the trend in metallicities between the H II regions of the four galaxies in our sample. As we found at least one valid detection of an auroral line in every one of our regions, we will not attempt to convert a metallicity abundance from any of our strong-line ratios. Instead, we will the plots of [O III] λ5007/Hβ and other strong-line ratios in Figure 3.3 to illustrate a trend in metallicity and temperature as a check on our direct method and far-infrared based derivations.

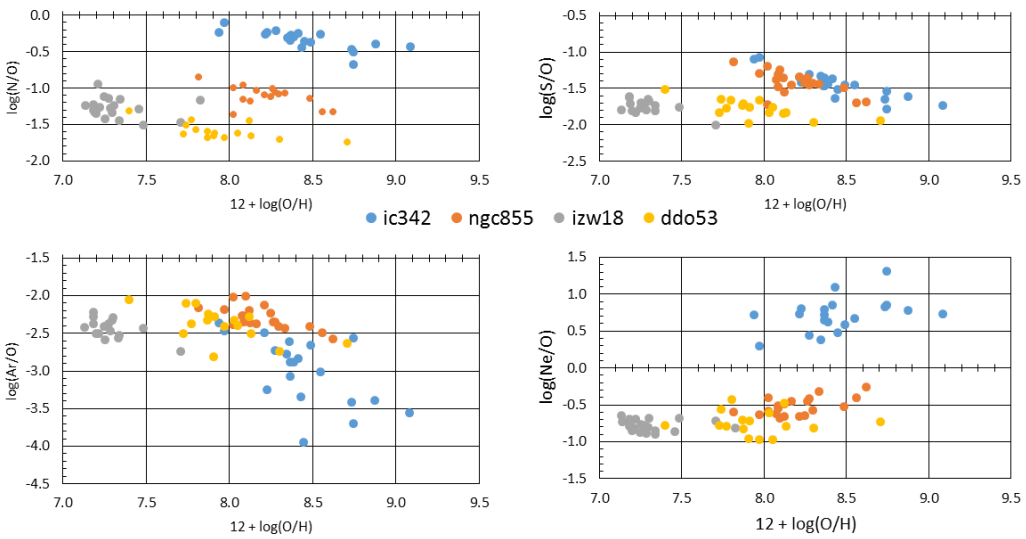

Fig. 3.2.— Nitrogen, sulfur, argon, and neon abundances plotted against oxygen for each region in our sample. I Zw 18 appears to have the most consistently measured metallicities. IC 342 shows some significant peculiarities, as many of its oxygen abundances are unusually low given its respective low temperatures, averaging around $12 + \log(\mathrm{O/H}) \sim 8.4$, and all of its neon abundances too high ($\log(\mathrm{Ne/O}) > 0$). Given the cool electron temperatures and heavy stellar contamination observed for IC 342, the neon abundances are not taken to be representative of the actual Ne/O ratio, and warrant further investigation.

	IC 342	NGC 855	I Zw 18	DDO 53
12 + log(O/H)	8.815 ± 0.070	8.153 ± 0.176	7.250 ± 0.136	7.807 ± 0.337
log(N/O)	-0.402 ± 0.013	-1.082 ± 0.061	-1.082 ± 0.074	-1.547 ± 0.101
log(Ar/O)	-3.544 ± 0.054	-2.325 ± 0.081	-2.264 ± 0.054	-2.340 ± 0.086
log(S/O)	-1.602 ± 0.046	-1.452 ± 0.059	-1.605 ± 0.051	-1.674 ± 0.094
log(Ne/O)	0.770 ± 0.041	-0.455 ± 0.081	-0.770 ± 0.053	-0.746 ± 0.137

Table 3.4. Abundances of the total combined spectra for NGC 855, I Zw 18, and DDO 53. IC 342 again is only composed of five selected regions (B I, C I, A IV, C IV, and E IV).

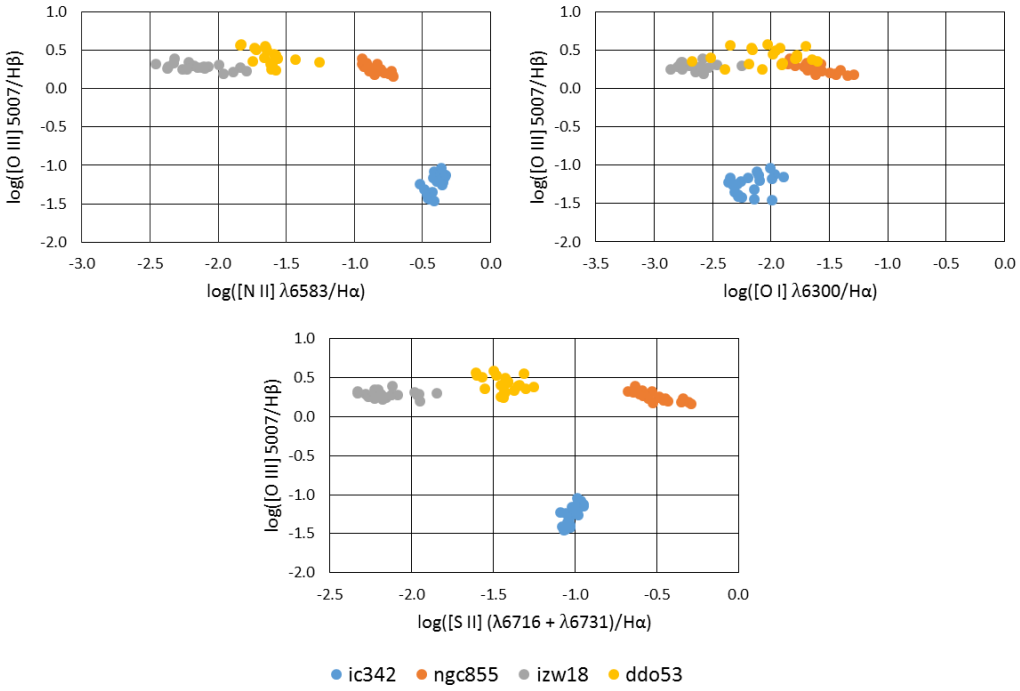

Fig. 3.3.— Plots of the strong-line ratios for every region in our sample. The curve traced out from I Zw 18 to IC 342 in the strong line ratios illustrates the trend from high to low temperature.

Chapter 4: Discussion and Conclusions

By combining observations from the LBT and Herschel KINGFISH survey, we derived gas-phase abundances for the H II regions of four galaxies that confirm our initial expectations that IC 342 and NGC 855 are cooler and more metal-rich compared to I Zw 18 and DDO 53.

Many of the regions in IC 342 when examined notably came out with oxygen abundances much lower than expected given the corresponding range of temperatures and the trend implied by the strong-line ratios. The large angular size of IC 342 meant that diffuse gas covered much of the galaxy in our observations, which may have suppressed accurate measurements of the weaker emission lines. IC 342 additionally exhibits a large of amount of extinction and heavy stellar contamination, which complicates measuring lines. This is also indicated by the unusually high neon abundances we find in every region of IC 342. A closer and more thorough examination of IC 342 will be necessary to properly resolve this discrepancy. However, as it is currently beyond the scope of this paper, we determined the metallicities for IC 342 through only using the five regions with a plausible oxygen abundance. As combining the total spectra still produced a low oxygen abundance, we instead summed the measured fluxes after model subtraction of each region to derive the metallicities, temperatures, and density for the galaxy. As the strong lines were unaffected by these peculiarities, we found the ratios in each region as normal and we used the [O III] λ5007 flux in total combined spectra with the [O III] μm line. This produced abundances close in agreement with the oxygen and nitrogen abundances found by Pilyugin et al. (2014).

The oxygen and nitrogen abundances found for DDO 53 fall within the same ranges as those reported by Berg et al. (2012). Our oxygen abundance for NGC 855, while somewhat lower than we might have expected given the stellar mass of the

galaxy and the detection of [O III] λ4363, is within the range of the low end value reported by Moustakas et al. (2010). The trend from I Zw 18 to IC 342 of low to high metallicity in the strong-line ratio plots are in agreement with the abundances we find through using the auroral lines.

We find that the abundances we calculate for I Zw 18 are relatively close to those previously reported (Skillman & Kennicutt 1993; Vilchez & Iglesias-Parama 1998; Lebouteiller et al. 2013) except in the case of nitrogen, where our abundance is higher by as much as over 0.50 dex. Skillman & Kennicutt (1993) provide one of the classic references for an optical determination of the oxygen abundance. Their oxygen abundance agrees with those of Vilchez & Iglesias-Paramo (1998), who similarly mapped I Zw 18 in the optical range, and Lebouteiller et al. (2013), who used the ultraviolet lines to measure the oxygen in the neutral ISM. Though the methodology Lebouteiller et al. (2013) is significantly different than those using optical observations of H II regions, the agreement of the abundances between Vilchez & Iglesias-Paramo (1998) and Lebouteiller et al. (2013) is strong evidence that our nitrogen abundance is aberrant and will require further investigation.

Our far-infrared temperature estimates proved to have smaller error ranges and demonstrate the same trend as temperatures found using the direct method for IC 342 and NGC 855. While the far-infrared and direct method temperature estimates are in agreement for NGC 855, the T[O III] value found using the 88 μm line for IC 342 was higher than expected. We find a pattern of systematically lower T[O III] estimates from the auroral lines for many regions in IC 342, I Zw 18, and DDO 53 compared to their respective T[S III] values. As discussed in Berg et al. (2015), in cases where there is a consistently large discrepancy between T[O III] and T[S III], the latter may be considered the more reliable temperature estimate. This appears to be true for IC 342, where our T[S III] measured using the auroral lines and converted from the far-infrared T[O III] values are in much closer agreement than the results of the two different methods for T[O III].

It is important to consider that the oxygen abundance for DDO 53 and, to a lesser extent, I Zw 18 both have overall large uncertainties in the far-infrared 88 μm line compared to IC 342 and NGC 855. This is likely a contribution of the low signal

from these metal-poor galaxies that can result from the fact that the temperature balance has not shifted as much power into the far-infrared lines. This is further implied by the temperature for DDO 53 being higher than that of I Zw 18, whereas the reverse is suggested by the direct and strong-line methods. For these galaxies, we will require more carefully generated Herschel maps of the far-infrared flux and error. We will also need to obtain a T[O III] estimate from the Herschel data before commenting on the accuracy of the high direct method T[S III] values for I Zw 18 and DDO 53.

This paper uses data taken with the MODS spectrographs built with funding from NSF grant AST-9987045 and the NSF Telescope System Instrumentation Program (TSIP), with additional funds from the Ohio Board of Regents and the Ohio State University Office of Research. This paper made use of the modsIDL spectral data reduction pipeline developed in part with funds provided by NSF Grant AST-1108693. This work was based in part on observations made with the Large Binocular Telescope (LBT). The LBT is an international collaboration among institutions in the United States, Italy and Germany. The LBT Corporation partners are: the University of Arizona on behalf of the Arizona university system; the Istituto Nazionale di Astrofisica, Italy; the LBT Beteiligungsgesellschaft, Germany, representing the Max Planck Society, the Astrophysical Institute Potsdam, and Heidelberg University; the Ohio State University; and the Research Corporation, on behalf of the University of Notre Dame, the University of Minnesota, and the University of Virginia. This research has made use of the NASA/IPAC Extragalactic Database (NED), which is operated by the Jet Propulsion Laboratory, California Institute of Technology, under contract with the National Aeronautics and Space Administration.

References

Aloisi, A., Clementini, G., Tosi, M., et al. 2007, ApJ, 667, L151

Berg, D. A., Croxall, K. V., Skillman, E. D., et al. 2015, arXiv:1501.02270

Bresolin, F., Garnett, D. R., & Kennicutt, R. C., Jr. 2004, ApJ, 615, 228

Bruzual, G., & Charlot, S. 2003, MNRAS, 344, 1000

Calzetti, D., Armus, L., Bohlin, R. C., et al. 2000, ApJ, 533, 682

Cid Fernandes, R., Mateus, A., Sodré, L., Stasińska, G., & Gomes, J. M. 2005, MNRAS, 358, 363

Croxall, K. V., Pogge, R. W., Berg, D., Skillman, E. D., & Moustakas, J. 2015, arXiv:1501.02272

Dalcanton, J. J., Williams, B. F., Seth, A. C., et al. 2009, ApJS, 183, 67

Dinerstein, H. L. 1990, The Interstellar Medium in Galaxies, 161, 257

Dopita, M. A., Kewley, L. J., Heisler, C. A., & Sutherland, R. S. 2000, ApJ, 542, 224

Fisher, D. B., Bolatto, A. D., Herrera-Camus, R., et al. 2014, Nature, 505, 186

Garnett, D. R. 1992, AJ, 103, 1330

Garnett, D. R., Kennicutt, R. C., Jr., & Bresolin, F. 2004, ApJ, 607, L21

Kennicutt, R. C., Calzetti, D., Aniano, G., et al. 2011, PASP, 123, 1347

Kewley, L. J., & Ellison, S. L. 2008, ApJ, 681, 1183

Kobulnicky, H. A., & Kewley, L. J. 2004, ApJ, 617, 240

Lebouteiller, V., Heap, S., Hubeny, I., & Kunth, D. 2013, A&A, 553, AA16

Moustakas, J., Kennicutt, R. C., Jr., Tremonti, C. A., et al. 2010, ApJS, 190, 233

Osterbrock, D. E., & Ferland, G. J. 2006, Astrophysics of gaseous nebulae and active galactic nuclei, 2nd. ed. by D.E. Osterbrock and G.J. Ferland. Sausalito, CA: University Science Books, 2006

Peimbert, M. 1967, ApJ, 150, 825

Pilyugin, L. S., & Thuan, T. X. 2005, ApJ, 631, 231

Pilyugin, L. S., Grebel, E. K., & Kniazev, A. Y. 2014, AJ, 147, 131

Pogge, R. W., Atwood, B., Brewer, D. F., et al. 2010, Proc. SPIE, 7735, 77350A

Saha, A., Claver, J., & Hoessel, J. G. 2002, AJ, 124, 839

Skillman, E. D., & Kennicutt, R. C., Jr. 1993, ApJ, 411, 655

Stasińska, G. 2002, Revista Mexicana de Astronomia y Astrofisica Conference Series, 12, 62

Tonry, J. L., Dressler, A., Blakeslee, J. P., et al. 2001, ApJ, 546, 681

Tremonti, C. A., Heckman, T. M., Kauffmann, G., et al. 2004, ApJ, 613, 898

Vílchez, J. M., & Iglesias-Páramo, J. 1998, ApJ, 508, 248